RSC Publishing Faraday Discussions

Spectral signatures of proton delocalization in $H^+(H_2O)_{n=1-4}$ ions

Journal:	*Faraday Discussions*
Manuscript ID	FD-ART-06-2018-000120
Article Type:	Paper
Date Submitted by the Author:	12-Jun-2018
Complete List of Authors:	McCoy, Anne; University of Washington, Chemistry Dzugan, Laura; The Ohio State University, Department of Chemistry DiRisio, Ryan; University of Washington, Chemistry Madison, Lindsey; University of Washington, Chemistry

Spectral signatures of proton delocalization in $H^+(H_2O)_{n=1-4}$ ions

Laura C. Dzugan,[†] Ryan J. DiRisio,[‡] Lindsey R. Madison,[‡] and Anne B. McCoy [*,‡]

Department of Chemistry and Biochemistry, The Ohio State University, Columbus, OH 43210, USA, and Department of Chemistry, University of Washington, Seattle, WA 98195, USA

E-mail: abmccoy@uw.edu

[*]To whom correspondence should be addressed
[†]Department of Chemistry and Biochemistry, The Ohio State University, Columbus, OH 43210, USA
[‡]Department of Chemistry, University of Washington, Seattle, WA 98195, USA

Abstract

Couplings involving large amplitude vibrations in $H^+(H_2O)_n$ (n = 1 - 4) are explored using several of theoretical approaches. These include harmonic treatments, analysis of harmonically coupled anharmonic oscillator (HCAO) models of the OH stretching vibrations, vibrational perturbation theory (VPT2) in internal coordinates, and diffusion Monte Carlo (DMC). It is found that couplings between the shared proton stretches and the HOH bends can lead to normal modes that are significantly mixed in character. The couplings among the various OH stretching vibrations are much weaker, and the OH stretches are well-described by harmonically coupled anharmonic oscillator models. Anharmonic couplings and the role of these large amplitude vibrations are further explored using DMC and VPT2. Based on the results of these calculations, it is found that all of the $H^+(H_2O)_n$ ions considered in this study display several different types of large amplitude vibrational motions even in their ground states. In the case of $H_7O_3^+$, degenerate VPT2 calculations indicate that there are large couplings between the shared proton stretch and various lower frequency vibrations that correspond to motions that break the ionic hydrogen bonds. This leads to vibrational eigenstates that have contributions from several zero-order states.

Introduction

Protons play a unique role in chemistry due their unusual properties in aqueous solution. In contrast to other ions, which exist as distinct chemical entities, excess protons move through the hydrogen bonded water network through a series of proton transfer events in which water molecules gain a proton and lose another. This is achieved through the Grotthuss mechanism,[1] and results in faster diffusion of protons in aqueous solution compared to other ions through a mechanism in which solvent fluctuations allow protons to be transferred between water molecules in a hydrogen-bonded network.[2–6]

The desire to understand the nature of proton mobility in solution has led to a number of theoretical, computational and experimental studies of the spectroscopy excess proton in both bulk water and in clusters.[7–15] These spectra have proven to be difficult to analyze due to the sensitivity of the frequency of the OH oscillator involving the transferring proton to the solvent environment. For example, considering only protonated water clusters with two to four water molecules, the frequency of the shared proton stretch ranges from from roughly 1000 cm^{-1} in $H_5O_2^+$[16,17] to more than 2500 cm^{-1} in $H_9O_4^+$.[15] All of these frequencies are significantly lower than the OH stretch frequency of water, which is roughly 3700 cm^{-1}[18] and the OH stretch frequency of an isolated hydronium ion, which is roughly 3500 cm^{-1}.[19] These observations are summarized in Table 1.

The above insights are based on a series of spectroscopic studies of protonated water clusters of various sizes.[10–12,15] While having the ability to measure the spectra of these clusters has proven an important advance in our understanding of the structure and proton mobility in these systems, attempts to analyze and assign these spectra using commonly available computational approaches have highlighted some of the limitations of these approaches.[16,20] The origin of the challenges for theoretical and computational spectroscopy is illustrated in the results reported in Table 1. In addition to the large range of OH stretch frequencies, the HOH bend frequency in protonated water dimer ($H_5O_2^+$) is significantly larger than the HOH bend frequencies in either water or hydronium.[21] In contrast, the HOH bend frequency in

$H_7O_3^+$ is lower than the corresponding frequencies of water and hydronium.[20] Finally studies of solvated protons have shown that features that are associated with ionic hydrogen bonding can span as much as 1000 cm^{-1}.[22,23] In those studies, we argued that this breadth can be qualitatively explained by recognizing that proton transfer is often accompanied by other structural changes.

In this work, we explore the connection between the position and breadth of features in the spectrum of protonated water clusters assigned to the shared proton stretch and bends based on a variety of theoretical and computational approaches. The goal is to illustrate the insights that can be obtained through the use of such a multifaceted approach to interpret the spectra. We also aim to obtain a better understanding of the manifestation of various types of couplings in the spectra of protonated water clusters.

Theory

In the present study, we explore several approaches for investigating large amplitude vibrations and the couplings involving these motions in protonated water clusters. These are systems that are formed when a hydronium ion is solvated by one or more water molecules. In the present work we focus on systems consisting of a hydronium ion in isolation and complexed with one to three water molecules. Unlike neutral water clusters, where the interactions among water molecules lead to modest shifts in the OH stretching and bending frequencies, the stronger intermolecular interactions in the protonated water clusters results in larger structural changes accompanied by modifications in the vibrational frequencies, as illustrated by the results presented in Table 1.

Harmonic Treatments

As we consider molecular vibrations, the most straightforward treatment involves describing the vibrations as $3N-6$ uncoupled harmonic oscillators, while the dipole surface is ap-

proximated by a linear function of these coordinates. Despite the relative simplicity of this approximation, harmonic treatments provide good zero-order descriptions of the physics for a broad range of molecular systems. This includes systems, like the protonated water clusters, which display large amplitude vibrations even in their ground states. The simplicity of harmonic models also makes them attractive approaches for investigating couplings in these systems.

Normal mode treatments of molecular vibrations have a long history.[24] In this approach, molecular vibrations are expressed as linear combinations of displacements of the coordinates of the atoms from their equilibrium configurations. The coordinates of choice are usually Cartesian coordinates as the normal mode coordinates can be defined as linear combinations of Cartesian displacements unambiguously. In this case, the kinetic energy is a function only of the Cartesian momenta and the masses of the atoms. Importantly, the kinetic energy does not depend on the molecular geometry. With this choice of coordinates, when the molecule is displaced along a normal mode, the atoms are constrained to follow Cartesian vectors. While this choice of underlying coordinates for defining the normal modes provides a good description of stretching vibrations, it results in a poorer description of bending motions. This can be seen in the the normal modes in $H_5O_2^+$ shown in Figure 1.

An alternative approach for defining the normal mode coordinates follows the description of Wilson.[24] In this case, the normal modes are constructed as linear combinations of internal coordinates (e.g. bond length, angles, and coordinates that describe internal rotations of the molecules). These coordinates are expected to provide an improved zero-order description of molecular vibrations compared to the Cartesian displacements, especially when large amplitude bending motions are involved.[25–27] The challenge with using internal coordinates to define the normal coordinates comes from the fact that unlike Cartesian coordinates the $3N-6$ internal coordinates are not uniquely defined. The size and nature of the couplings among the vibrations is sensitive to the choice of internal coordinates. Additionally, by using $3N-6$ internal coordinates, the kinetic energy will depend on the molecular geometry as

well as the masses of the atoms and the momenta conjugate to the chosen set of coordinates.

Independent of the choice of coordinates, the normal mode analysis is performed by first expressing the Hamiltonian in terms of a set of coordinates ($3N$ Cartesian coordinates or $3N-6$ internal coordinates) as[24]

$$\hat{H} = \frac{1}{2}\sum_{i,j}\left[p_{s,i}G_{i,j}p_{s,j} + \frac{\partial^2 V}{\partial s_i \partial s_j}(s_i - s_{i,e})(s_j - s_{j,e})\right] \tag{1}$$

where $(s_i - s_{i,e})$ represents the displacement of one of the coordinates from its equilibrium value, $p_{s,i}$ is the momentum conjugate to s_i, and $G_{i,j}$ is an element of the Wilson **G**-matrix. If Cartesian coordinates are used the

$$G_{i,j}^{\text{cart}} = \frac{1}{m_i}\delta_{i,j}, \tag{2}$$

where m_i represents the mass of the atom that is being displaced. In general, the **G**-matrix elements are functions of the coordinates of the atoms. Expressions for the **G**-matrix elements can be obtained from tabulations[24,28] or by evaluating

$$G_{i,j}^{\text{int}} = \sum_{n=1}^{3N}\frac{\partial r_i}{\partial x_n}\left(\frac{1}{m_n}\right)\frac{\partial r_j}{\partial x_n} \tag{3}$$

The normal mode analysis is performed by first defining a set of mass-weighted coordinates

$$s_i' = \sum_j \left(G^{-1/2}\right)_{i,j}(s_j - s_{j,e}) \tag{4}$$

The Hamiltonian, when expanded through second order in these coordinates and their conjugate momenta, becomes

$$\hat{H} = \frac{1}{2}\sum_i p_{s',i}^2 + \frac{1}{2}\sum_{i,j} s_i' F_{i,j} s_j' \tag{5}$$

where $F_{i,j}$ represents an element of the Hessian, evaluated in terms of these mass-weighted

coordinates. The eigenvalues of $\mathbf{F}$ provide the squares of the harmonic frequencies, ω_n^2, while the eigenvector matrix, $\mathbf{T}$, provides the transformation between the normal modes and s'. Finally, the transformation between initial displacement coordinates and the normal coordinates is defined as

$$\begin{aligned}(s_j - s_{j,e}) &= \sum_k \sum_n \left(G^{1/2}\right)_{j,k} T_{k,n} \omega_n^{-1/2} Q_n \\ &= \sum_n \mathcal{L}_{j,n} Q_n \end{aligned} \tag{6}$$

while

$$p_j = \sum_n \left(\mathcal{L}^{-1,T}\right)_{j,n} P_{Q,n} \tag{7}$$

and the corresponding Hamiltonian through quadratic terms in the coordinates and conjugate momenta is

$$\hat{H} = \frac{1}{2} \sum_n \left[\omega_n \left(p_{Q,n}^2 + Q_n^2\right)\right] \tag{8}$$

In some cases it can be advantageous to consider a local mode treatment of molecular vibrations. This is particularly true in the case of large amplitude anharmonic OH stretching vibrations where the anharmonicity of the potential along the OH stretch coordinate has a larger influence on the vibrational energy level pattern than the couplings among the OH oscillators. An example of this effect can be seen in the overtones of H_2O,[18] where the state that is assigned as having two quanta in the symmetric stretch ($|2,0,0\rangle$) is 50 cm^{-1} lower in energy than the combination band with one quantum in each the symmetric and antisymmetric stretch ($|1,0,1\rangle$), while the combination band is 200 cm^{-1} lower in energy than the $|0,0,2\rangle$ state. Here we use a notation in which states are described in terms of the number of quanta in the symmetric stretch, n_s, the number of quanta in the bend, n_b, and the

number of quanta in the asymmetric stretch, n_a, as $|n_s, n_b, n_a\rangle$. For states with three quanta in the stretches, the $|3,0,0\rangle$ and the $|2,0,1\rangle$ states are split by 14 cm^{-1}, and the $|1,0,2\rangle$ and $|0,0,3\rangle$ states are split by 164 cm^{-1}, while the two pairs of states are split by more than 250 cm^{-1}.[18] In a harmonic picture one would expect evenly spaced energy levels, where the energy difference is determined by the difference between the frequencies of the symmetric and antisymmetric stretch, which is approximately 100 cm^{-1} for water. The observed pattern suggests that these oscillators are better described in a local mode representation where the pairs of nearly degenerate states are identified as in- and out-of-phase combinations of local mode stretches, denoted as $|n_1, n_2\rangle_{\pm}|n_b\rangle = |n_1, n_2, n_b\rangle \pm |n_2, n_1, n_b\rangle$, where n_1 and n_2 indicate the number of quanta in each of the two localized OH stretch. In this notation, the $|2,0,0\rangle$ and $|1,0,1\rangle$ normal mode states become the in- and out-of-phase combinations of the local mode states with two quanta in a single OH oscillator $|2,0\rangle_{\pm}|0\rangle$, while the $|0,0,2\rangle$ state corresponds to a state with one quantum in each oscillator in the local mode picture, $|1,1\rangle|0\rangle$.

Lehmann, Childs, Mills and others[29–31] have explored the connections between these models and proposed a harmonically coupled anharmonic oscillator picture to describe OH stretching vibrations (q_n) in which

$$H = \frac{1}{2}\sum_n \left[\omega_n \left(p_{q,n}^2 + q_n^2\right) + \sum_j F_n^{(j)} q_n^j\right] + \sum_{n>m} f_{n,m}\left(a_n^\dagger a_m + a_n a_m^\dagger\right) \tag{9}$$

where a_n and $a_n^\dagger$ represent harmonic raising and lowering operators. We have used this model in several recent studies of the spectra of molecules that contain coupled XH oscillators.[32–34] For the OH stretches of the hydronium core in protonated water clusters, the strong ionic hydrogen bonds make the diagonal anharmonicity of these OH oscillators particularly large, and an anharmonicly coupled harmonic oscillator model is expected to be more appropriate for describing these vibrations than the harmonic description.

Following the work of Sibert,[35] we have generated linear combinations of the normal modes that correspond to the OH stretch vibrations, $\mathbf{Q}_R$, which are constructed so that they

involve the motion of a single OH oscillator.

More specifically, we begin by defining a set of dimensionless local modes for the OH stretches, $\{\mathbf{q}_R\}$. If the normal modes are described in terms of internal coordinates,

$$q_{R,n}^{\text{int}} = \sqrt[4]{\frac{1}{\mu_n F_{nn}}}(s_n - s_{n,e}) \tag{10}$$

where F_{nn} is the diagonal quadratic force constant for that OH oscillator, and μ_n represents the corresponding reduced mass. When the normal modes are defined as linear combinations of Cartesian displacements, each of the $q_{R,n}$ is obtained by performing a normal mode calculation for the ion under investigation in which the masses of all of the atoms except the two that make up the OH bond are multiplied by a factor of 10. In this case,

$$q_{R,n}^{\text{cart}} = \mathcal{L}_{n,j}^{-1}\left(s_j - s_{j,e}\right) \tag{11}$$

This calculation is repeated for each of the OH oscillators, and we use $\mathcal{L}_{LR}$ to represent the transformation between the displacement of the internal or cartesian coordinates and the q_R coordinates. Additionally

$$\mathbf{Q}_R = \mathcal{L}_R^{-1}\left(\mathbf{s} - \mathbf{s}_e\right), \tag{12}$$

where $\mathcal{L}_R^{-1}$ represents the rows of the $\mathcal{L}^{-1}$-matrix that correspond to the OH stretch normal modes. We can combine the above relationships to obtain

$$\mathbf{q}_R = \mathcal{L}_{LR}^{-1}\mathcal{L}_R\mathbf{Q}_R \equiv \mathbf{A}\mathbf{Q}_R \tag{13}$$

As $\mathbf{A}$ is not orthogonal, in the spirit of Löwdin orthogonalizaiton, Sibert and co-workers[35] define $\mathbf{O} = \mathbf{A}^T\mathbf{A}$, and construct a set of localized coordinates as

$$\mathbf{q}'_R = \mathcal{L}_{LR}^{-1}\mathcal{L}_R\mathbf{O}^{-1/2}\mathbf{L}_R^{-1}\left(\mathbf{s} - \mathbf{s}_e\right) \equiv \mathcal{L}_{LRO}^{-1}\left(\mathbf{s} - \mathbf{s}_e\right) \tag{14}$$

With these coordinates in place, the harmonic Hamiltonian takes the form of Eq. 9, providing us with the opportunity to explore the nature and strength of couplings both among the OH oscillators and between the OH oscillators and other vibrational degrees of freedom.

Beyond harmonic treatments

As we consider extensions beyond the harmonic treatments a natural next step is second order vibrational perturbation theory (VPT2). In contrast to more general perturbation theory approaches, in the vibrational treatment the Hamiltonian is expanded in powers of λ, along with the energies and wave functions.[26,36] This follows from the fact that the logical corrections to the Hamiltonian that is a quadratic expansion in coordinates and momenta is to introduce cubic and higher order terms in the expansion. Based on this, terms that are cubic in the coordinates and momenta are introduced in $H^{(1)}$ while quartic terms contribute to $H^{(2)}$, leading to

$$H = H^{(0)} + \lambda H^{(1)} + \lambda^2 H^{(2)} + \cdots \tag{15}$$

Since the kinetic energy is quadratic in the momentum, $H^{(1)}$ includes cubic terms of the form $p_i \left[(\partial G_{i,k}/\partial Q_j)\, Q_j \right] p_k$ and terms that involve third derivatives of the potential function. In the absence of degeneracies, the energy expressions will take the form of expansions in powers of $(n_m + 1/2)$ with linear terms contributing to $E^{(0)}_{\mathbf{n}}$, and quadratic terms in $(n_m + 1/2)$ as well as a scalar shift to the zero-point energy contribute to $E^{(2)}_{\mathbf{n}}$. By symmetry, $E^{(1)}_{\mathbf{n}} = 0$.

As with all calculations based on perturbation theory, small differences in the energies of zero-order states can become problematic. Martin and co-workers[37] developed an approach for determining when near degeneracies need to be accounted for. This is achieved by evaluating the contribution from coupling to a selected zero-order state to the energy of the state of interest. Specifically, if the state of interest is $|\Psi_n\rangle$ and we are considering the role of coupling to $|\Psi^{(0)}_m\rangle$, where $\langle \Psi^{(0)}_n | H^{(1)} | \Psi^0_M \rangle = W$, we evaluate the contribution to the energy

by two approaches. Following Martin, in the first, we determine the eigenvalues of a reduced dimensional Hamiltonian matrix in the basis of these two states:

$$H = \begin{pmatrix} E_n^* & W \\ W & E_m^* \end{pmatrix} \tag{16}$$

where E_n^* represents the energy of a state calculated using second order perturbation theory when the contribution from $|\Psi_m^{(0)}\rangle$ is not included in the first order correction to $|\Psi_n\rangle$, and E_m^* is evaluated in an analogous manner. These eigenvalues are compared to the value of the energy, evaluated through second order in perturbation theory, including the contribution from $|\Psi_m^{(0)}\rangle$. Following Martin, the differences between these energies provides a measure of the anharmonicity effect, γ, where

$$\gamma = \frac{\left|\langle\Psi_m^{(0)}|H^{(1)}|\Psi_n^{(0)}\rangle\right|^4}{\left(E_n^{(0)} - E_m^{(0)}\right)^3} \tag{17}$$

if $\gamma \geq 1$ cm^{-1} we consider the states to be strongly coupled and treat these couplings using degenerate perturbation theory.[38,39]

As with the harmonic treatments, VPT2 may be implemented for a variety of definitions of the normal modes. In the absence of resonances, the resulting energies will be independent of this coordinate choice.[27] On the other hand, when there are degeneracies, or near degeneracies, the results can become quite sensitive to this choice, and generally normal modes based on linear combinations of internal coordinates will provide better convergence of the expansion of the potential function as well as the **G**-matrix elements than those based on Cartesian displacements. A description of our implementation of degenerate VPT2 can be found elsewhere.[38,39]

Diffusion Monte Carlo

In Diffusion Monte Carlo,[40–43] the wave function is described by an ensemble of localized functions, called walkers, which are allowed to diffuse in the $3N$ dimensional space that represents possible geometries of the molecule of interest. The diffusion is based on the action of the imaginary time, time-dependent Schrödinger equation on this ensemble,

$$\exp\left\{-\left(H-E_{\mathrm{ref}}\right)\tau\right\}\prod_{j=1}^{n_{\mathrm{walkers}}} f((\mathbf{x}-\mathbf{x}_j) \approx \prod_{k=1}^{n_{\mathrm{steps}}} \exp\left\{-\left(V-E_{\mathrm{ref}}\right)\Delta\tau\right\}\exp\left\{-T\Delta\tau\right\} \times \prod_{j=1}^{n_{\mathrm{walkers}}} f((\mathbf{x}-\mathbf{x}_j) \quad (18)$$

Here, $f((\mathbf{x}-\mathbf{x}_j)$ represents one of the localized walkers, which is centered at $\mathbf{x}_j$, while $\tau = it/\hbar$ and E_{ref} is introduced to keep the amplitude of the wave function constant. In the long-time limit, the solution to Eq. 18 becomes

$$\begin{aligned}\lim_{\tau\to\infty}\exp\left\{-\left(H-E_{\mathrm{ref}}\right)\tau\right\}\Psi(x,\tau) &= \sum_n c_n \exp\left\{-\left(E_n-E_{\mathrm{ref}}\right)\tau\right\}\phi_n(\mathrm{x}) \\ &= c_0\exp\left\{-\left(E_0-E_{\mathrm{ref}}\right)\tau\right\}\phi_0(\mathrm{x}) \quad (19)\end{aligned}$$

where ϕ_n represents an eigenstate of H, with corresponding energy E_n. By rotating to imaginary time, the oscillatory phase factors are replaced by exponentially decaying functions, and in the long-time limit, the contribution from the lowest-energy state will dominate the expansion in Eq. 19. In the case where $E_{\mathrm{ref}} = E_0$, the contribution from this state will be constant. Since E_0 is an unknown, the value of E_0 is determined by varying E_{ref} so that $\Psi(\tau)$ has constant amplitude, as described in more detail in the discussion that follows.

More specifically, the DMC simulations are performed by propagating Ψ over a series of small time steps with $\Delta\tau = 1$ to 10 a.u. During each time step, each of the coordinates of each of the walkers is displaced by a random amount based on a Gaussian distribution with

$\sigma_i^2 = \Delta\tau/m_i$,[40] where m_i is the mass associated with the ith Cartesian coordinate. After the coordinates of a walker have been displaced, the potential energy is evaluated at the new geometry, and the value of

$$P_j(\tau) = \exp\left\{-\left(V(\mathbf{x}_j(\tau)) - E_{\text{ref}}\right)\Delta\tau\right\} \tag{20}$$

is used to determine the number of walkers that are localized at $\mathbf{x}_j$ at the start of the next time step. Specifically, the integer value of P_j provides the number of walkers at these coordinates, and $[P_j - \text{Int}(P_j)]$ is compared to a random number taken from a uniform distribution between 0 and 1 to determine if an additional walker will be introduced at these coordinates. At the end of the time step, E_{ref} is evaluated using[41]

$$E_{\text{ref}} = \overline{V}(\tau) - \alpha\left[\frac{N(\tau) - N(\tau = 0)}{N(\tau = 0)}\right] \tag{21}$$

where $N(\tau)$ provides the number of walkers at time τ and α is a simulation parameter. In the current work we we use[44]

$$\alpha = \frac{1}{2\Delta\tau} \tag{22}$$

We equate E_0 to the average value of E_{ref} over a large number of $\Delta\tau$, after the simulation has equilibrated. The density of walkers can be used to obtain the corresponding wave function, $\Psi_0(\mathbf{x})$.

To obtain other properties, for example $\langle x\rangle$, or projections of Ψ_0^2 onto a specific coordinate, we need an independent approach for evaluating the value of Ψ_0 at the coordinates of the walkers as for the multiplicative operator, A,

$$\langle A\rangle = \int \Psi_0^2(\mathbf{x})A(\mathbf{x})d\mathbf{x} = \sum_j \Psi_0(\mathbf{x}_j)A(\mathbf{x}_j) \tag{23}$$

by Monte Carlo integration.[42] To find the value of $\Psi(\mathbf{x}_j)$, we exploit the fact that each of

our localized functions can be expanded as a linear superposition of the eigenstates of the Hamiltonian for the system of interest as[45]

$$f_i(\mathbf{x} - \mathbf{x}_j(\tau_0)) = \sum_n c_{i,n}(\tau_0)\phi_n(\mathbf{x}) \tag{24}$$

where $c_{i,n}(\tau_0) = \phi_n(\mathbf{x}_i(\tau_0))$. Based on the above discussion, after propagating an ensemble of these functions forward in time only the contribution from ϕ_0 survives, and we can equate the number of walkers in the ensemble at some time later that can be traced back to the ith walker at τ_0, d_i, to the value of $\phi_0(\mathbf{x}_i(\tau_0))$. These d_i's are often referred to as the descendent weights of the ith walker. Replacing $\Psi_0(\mathbf{x}_j)$ with d_j in Eq 23, we are able to evaluate expectation values of any multiplicative operator. This also allows us to project the probability amplitude onto any coordinate of interest.

Numerical Details

In the present DMC simulations, we have used the potential surfaces for protonated water clusters developed by Bowman and co-workers.[20,46] We propagated roughly 20 000 walkers for 40 000 time steps of 10 a.u. each. Starting at 5000 time steps, the wave functions are collected after every 1000 time steps. Probability amplitudes are evaluated based on collecting desendants from each of these wave functions for an additional 20 time steps. The descendent weighting calculations were repeated 35 times and the results are averaged to improve the accuracy. For the harmonic calculations, we use single point calculations and harmonic force fields obtained from electronic structure calculations performed at the MP2/aug-cc-pVTZ level of theory using the Gaussian 16[47] program package for the exploration of couplings among the OH stretches and at the MP2/aug-cc-pVDZ level of theory using Gaussian 09[48] for the study of stretch bend couplings. Finally, for the remainder of the discussion we take $\hbar = 1$.

Results and Discussion

Vibrationally Averaged Structures

We begin by focusing on the structures of the protonated water clusters. In particular we investigate the extent to which these ions explore higher symmetry configurations when they are in their vibrational ground states. Based on previous studies of hydronium[49,50] and $H_5O_2^+$[51,52] the ground state wave functions for both of these ions have significant amplitude near configurations that correspond to transition states for large amplitude torsion and umbrella motions, shown in the lower panel of Figure 2. For comparison, the equilibrium structures are provided in the upper panel of this figure. In H_3O^+ the higher symmetry structure corresponds to the transition state in the umbrella inversion vibration. Likewise, the vibrationally averaged structure of $H_5O_2^+$ has D_{2d} symmetry with the two flanking water molecules lying in planes perpendicular to the OO axis and in planes perpendicular to each other. For the larger systems, the transition states correspond to the hydronium core as well as the oxygen atoms in the flanking water molecules lying in a plane, with the flanking water molecules oriented perpendicular to this plane.

These results are illustrated by the plots of the projections of the probability amplitude, calculated using DMC, shown in Figure 3(a). To evaluate these projections, for each of the walkers we determined the value of the out-of-plane bending coordinate, θ_{oop}. This angle is evaluated by first defining a plane that contains the termini of unit vectors that lie along the three OH or OO bonds originating from one of the oxygen atoms. A vector normal to this plane is constructed. θ_{oop} is the angle between this normal vector and any one in the unit vectors along the OH or OO bonds. It should be noted that the above definition ensures that all three possible definitions of θ_{oop} result in identical values. This definition of θ_{oop} is illustrated for H_3O^+ in Figure 4. While for H_3O^+ the choice of the vectors used to define θ_{oop} is unambiguous, for the larger clusters, we use the OO bonds connected to the central oxygen atom along with any free OH bonds. For example in $H_5O_2^+$, θ_{oop} is defined in terms

of the two OH bonds in a flanking water molecule along with the OO bond.

As is seen in Figure 3(a), $\theta_{oop} = 90°$ in the transition state geometries, and has maxima at $\theta_{oop} \approx 75°$ and 135°. These most probable values of θ_{oop} are close to the equilibrium values of θ_{oop} for these ions, which are found to range from 72.6° to 76.7° when the geometries are optimized at the MP2/aug-cc-pVTZ level of theory.

As these projections indicate, the probability amplitude near the transition state is significant. It is roughly half the maximum amplitude in H_3O^+ (green line in Figure 3(a)) for which the barrier along this coordinate is roughly 700 cm^{-1}.[49] This large probability amplitude at the transition state is also consistent with the reported ground state tunneling splitting in H_3O^+ of 55 cm^{-1}.

When a second water molecule is introduced, there are now two types of large amplitude bending motions. The first is the tunneling motion described above. The torsion motion involving the two flanking water molecules provides a second large amplitude motion. This is illustrated in Figure 3(b). Here the torsion angle, ϕ, is defined as the angle between the projections of the bisectors of the HOH angles of the two flanking water molecules that are perpendicular to the OO axis. In the case of the umbrella tunneling coordinate in $H_5O_2^+$, the relevant transition state is 164 cm^{-1} above the potential minimum.[49] This lower barrier is consistent with roughly equal probability amplitude at $\theta_{oop} = 90°$ and at the potential minimum, shown with the green curve in Figure 3(a). In the case of the projection of the probability amplitude onto ϕ shown in Figure 3(b), the distribution has finite amplitude at all values of this coordinate, and the largest amplitude is found near 90°. This is consistent with the barrier for planarity of one of the flanking water molecules of 158 cm^{-1} while the barrier for 180° rotation of one of the water molecules is 213 cm^{-1}.[49]

Introducing additional water molecules leads to analogous behavior. For $H_7O_3^+$, the probability amplitude at θ_{oop} at 90° is intermediate between the values found for $H_5O_2^+$ and H_3O^+ while the value for $H_9O_4^+$ is similar to that for H_3O^+. To further explore the amplitude of these out-of-plane motions, we plot the projections of the probability amplitude onto the

coordinates that correspond to the signed distance of the hydrogen atoms from the plane that contains three of the oxygen atoms, defined as z. While for $H_7O_3^+$ there are only three oxygen atoms, for $H_9O_4^+$ we define the OOO plane using the three oxygen atoms that are contained in the flanking water molecules. In this case, z is defined so the central oxygen atom has $z \geq 0$. To simplify the plots, we have averaged the probability distributions for equivalent hydrogen atoms.

For $H_7O_3^+$ there are three unique types of hydrogen atoms, while there are only two in $H_9O_4^+$. In both molecules the probability distributions for the bonded hydrogens, shown with blue curves in Figure 3(c) and (d), is narrow. In $H_7O_3^+$ this distribution is peaked at the origin, while it is peaked at $z = 0.2$ Å in $H_9O_4^+$. The shift of the position of this peak in the larger ion reflects the fact that the oxygen atom in hydronium is defined to have $z \geq 0$. With nearly collinear O-H$\cdots$O hydrogen bonds, the hydrogen atoms involved in hydrogen bonding will also lie slightly above the plane that contains the remaining three oxygen atoms.

In $H_7O_3^+$ there is also a free OH bond to the hydronium core. The probability distribution for displacements of this atom from the plane containing three oxygen atoms plotted with the red curve in Figure 3(c) shows similar structure to the tunneling in Figure 3(a) as is expected because it represents the same motion. The probability distributions plotted with green lines provide the displacements of the hydrogen atoms in the flanking water molecules. These distributions are bimodal, reflecting the large amplitude rotational motions of the flanking water molecules. This is entirely analogous to the large amplitude motions along ϕ seen for $H_5O_2^+$, plotted in Figure 3(b). By analogy to H_3O^+ and $H_5O_2^+$, these distributions indicate that the vibrationally averaged structures for these larger clusters resemble those shown in the lower panels of Figure 2.

Harmonic Stretch/Bend Couplings

With the vibrationally averaged structures in hand, we now explore the harmonic contributions to mode mixing. For this analysis, it is convenient to focus on the higher symmetry

transition state structures as they simplify the description of the couplings. Using these structures also makes the definitions of the intramolecular coordinates transferrable among the different sized ions. Specifically, the internal coordinates are defined as linear combinations of the various OH and OO distances, linear combinations of the HOH angles for the hydronium core and the OOO angles as well as linear combinations of the OOH angles involving the hydrogen atoms in the flanking water molecules. While the HOH bends for the flanking water molecules are not included in this list of internal coordinates, this motion is fully described by the appropriate linear combination of the OOH angles.

A harmonic representation of the Hamiltonian is constructed in terms of symmetry adapted linear combinations of these coordinates as

$$H = \frac{1}{2} \sum_{i,j} \left[p_{t,i} G_{ij}^{\mathrm{sym}} p_{t,j} + t_i F_{ij}^{\mathrm{sym}} t_j \right] \tag{25}$$

where $\{t_i\}$ represent the symmetry adapted linear combinations of displacements of internal coordinates, while $\{p_{t,i}\}$ are the momenta conjugate to these coordinates. The kinetic couplings are captured in the off-diagonal elements of the Wilson **G**-matrix, G_{ij}^{sym}, while the F_{ij}^{sym} provide the potential couplings. To simplify the discussion that follows, we use dimensionless coordinates and momenta, where the linear combinations of the displacement coordinates have been scaled by $\sigma_i = \sqrt[4]{F_{ii}^{\mathrm{sym}}/G_{ii}^{\mathrm{sym}}}$ while the momenta area scaled by $1/\sigma_i$. The results of this analysis are provided in Table 2.

As is seen in these results, for H_2O, the kinetic and potential couplings are both large, and they have opposite signs. This leads to a partial cancelation of their contributions. It should be noted that while the signs of the coupling terms depend on how the $t-$coordinates are constructed, the relative signs of the kinetic and potential couplings are meaningful. The large frequency difference between the local in-phase (symmetric) OH stretch and the bend leads to a modest shift in the frequency when these couplings are introduced. This can be seen by the fact that the coupled and uncoupled frequencies reported in Table 2 differ by less than 20 cm^{-1}. For water and all the other systems, uncoupled frequencies are equivalent to

the values of F_{ii} and G_{ii}, which are equal in these dimensionless coordinates. The coupled frequencies are those obtained through a reduced-dimensional FG-analysis,[24] which is based on the shared proton stretch, the free OH stretches as well as the HOH bends. The reported coupling terms are the values of $F_{i,j}^{\mathrm{sym}}$ and $G_{i,j}^{\mathrm{sym}}$ in Eq. 25. For comparison the frequencies from a full-dimensional normal mode calculation are provided in Tables S1-S3.

In H_3O^+, the potential coupling is smaller than in H_2O, while the kinetic coupling has increased. This reflects the larger HOH angle in the saddle point structure of H_3O^+ (120°) compared to the HOH angle in water (104.1°). As with H_2O, the shifts in the harmonic frequencies with the introduction of stretch/bend coupling is small.

The situation changes for $H_5O_2^+$, where the potential coupling is twice as large as in H_2O, and nearly a factor of 20 larger than in H_3O^+. In this molecule, the kinetic couplings are small. Further, the uncoupled bend frequency is comparable to those in H_2O and H_3O^+. In fact the frequency of the uncoupled HOH bend ranges rom 1616 to 1655 cm^{-1} across all the systems considered here. In contrast, the harmonic frequency of the shared proton stretch, which corresponds to the motion of the shared proton parallel to the OO axis, is significantly red shifted and is now 600 cm^{-1} below the bend frequency rather than nearly 2000 cm^{-1} above the bend frequency, as was found for the two previous systems. With these observations in hand when the stretches and bends are allowed to mix the larger differences between the uncoupled and coupled frequencies are found. Likewise, as reported in Table S1, the intensity of this bend fundamental is increased from 119 to 1600 km mol^{-1}, reflecting the highly mixed nature other shared proton stretch and out-of-phase HOH bends when the normal modes are constructed. This results addresses one of the observations noted above regarding the surprisingly high bend frequency and intensity seen in the spectrum of $H_5O_2^+$.

Deuteration reduces the size of the effective couplings due to the use of dimensionless coordinates. As a result, deuterating either of the outer water molecules or the shared proton will decrease the size of the coupling by roughly a factor of $\sqrt[4]{2}$, while deuteration of both the shared proton and the outer water molecules decreases the stretch/bend coupling by a factor

of $\sqrt{2}$. This leads to smaller stretch/bend coupling in $D_5O_2^+$ compared to $H_5O_2^+$. When only the outer water molecules are deuterated, the energy difference between the local shared proton stretch and bend is reduced to 70 cm^{-1}. This splitting is 880 cm^{-1} when the shared proton is deuterated, while there are hydrogen atoms in the outer water molecule. This leads to a significant frequency shift and increase in the intensity of the of the DOD bends when H^+ is shared between two DOD molecules, while the mixing is not as pronounced when D^+ is shared by two HOH molecules. It also leads to the bend fundamental having greater intensity at the harmonic level compared to the shared proton stretch in $H^+(D_2O)_2$. The above results are summarized in Tables 3 and S1. The conclusions are consistent with those reported previously and with the measured spectra of these ions.[21,52]

As we move to $H_7O_3^+$, there are now two types of HOH bends that are coupled to the shared proton stretch. These involve the HOH bends of the hydronium core and the HOH bends of the water molecule. Taken together, there are four bending and two stretching vibrations. When symmetry is introduced, two sets of three vibrations remain coupled. The kinetic coupling between the shared proton stretch and the bends of the flanking water molecules is rigorously zero as the two motions do not involve any common atoms. The kinetic couplings between the shared proton stretch and the bends in the hydronium core are comparable in magnitude to the couplings in water and 75% the size of the stretch/bend kinetic couplings in hydronium. In both cases, though, the kinetic coupling is smaller than the corresponding potential coupling. In comparison to $H_5O_2^+$, the stretch bend couplings are weaker, and the energy difference between the uncoupled harmonic frequencies for the stretch and the bend are larger. In addition, the shared proton OH stretch is higher in frequency than the bend. The coupling of these vibrations leads to red shifts in frequency of the bend fundamental, the magnitude of which is smaller than in $H_5O_2^+$, but larger than in water or hydronium. In contrast to $H_5O_2^+$ where the stretch bend couplings lead to substantial increases in the intensity of the bend fundamentals, the intensity of the bend fundamentals in $H_7O_3^+$ are surpressed by a factor of two when it is coupled to the shared proton stretch.

This is seen in the results reported in Table S2. This decrease in the intensities of the bend fundamentals in strongly hydrogen bonded systems has been attributed to a cancelation of mechanical (motion of hydrogen atoms that have positive partial charges) and electrical (the decrease of these partial charges when the hydrogen bonds are weakened through the HOH bending motions), and when coupled to the shared proton stretch the contributions to the transition moments from the local stretch and bend vibrations partially cancel for the normal modes that have primarily bending character.[53] Some of this intensity is recovered when higher order terms are included in the Hamiltonian. These terms will lead to a redshift of the frequency of the shared proton stretch, making it closer to that of the bend fundamental. The higher order terms provide additional couplings between the shared proton stretch and the bend.

These trends continue for $H_9O_4^+$, where the shared proton stretch has shifted to even higher frequency leading to smaller shifts in the frequencies of the uncoupled vibrational frequencies upon coupling. Once again, the intensity of the bend is decreased with coupling to the shared proton stretch.

Since it is difficult to sort out contributions from kinetic and potential coupling terms in the Hamiltonian, we have repeated the analysis, setting the kinetic coupling to zero. The results are also reported in Tables 2 and 3. In all cases the frequency shifts with and without consideration of kinetic couplings are comparable to each other and to the results obtained from a full normal mode treatment (reported in Tables S1-S3). This allows us to attribute the leading contribution to the large mixing of the shared proton stretch and the HOH bends, particularly in $H_5O_2^+$, to the potential surface rather than to couplings in the kinetic energy terms in the Hamiltonian.

Couplings among the OH stretches

We next turn our attention to the coupling among the OH stretches, which is notably weaker than the stretch/bend couplings discussed above. Here we focus on the results from

the localized treatments described above. Although these couplings are also encoded in the normal mode description used to explore the stretch/bend couplings, the collective nature of the vibrations in that treatment makes the trends more difficult to sort out.

In Table 4, we report the values of the couplings among the local OH stretches for systems ranging from an isolated water molecule up through $H_9O_4^+$. Consistent with the splittings between the symmetric and antisymmetric stretches in water the calculated coupling, evaluated at the MP2/aug-cc-pVTZ level of theory/basis set, is found to be 63 cm^{-1}. This coupling is reduced to 36.5 cm^{-1} in hydronium. The smaller coupling in hydronium reflects the fact that each of the OH oscillators in hydronium is coupled to two other OH vibrations, while there are only two OH oscillators in water. As such, extending one of the OH bonds in hydronium has a smaller effect on the force experienced by each of the other oscillators in hydronium compared to water. When a water molecule is hydrogen-bonded to hydronium, the stretch-stretch coupling drops to a value that is intermediate to the corresponding values for hydronium and water. Interestingly there is little variation in the value of this parameter for the three protonated hydronium clusters studied here.

In contrast, the coupling between the hydrogen bonded OH stretch in $H_5O_2^+$ and the OH stretches in the flanking water is nearly 100 cm^{-1}. This large coupling reflects the fact that as the central proton is displaced the system moves to resemble a hydronium ion solvated by a single water molecule. As the OH bond lengths in hydronium are larger than those in water (see Table 1), this motion is accompanied by the elongation of the OH bonds on one of the flanking water molecules and a contraction of the OH bond lengths on the other.

The effects of this coupling are also seen in $H_7O_3^+$, although the strength of the coupling is diminished. In addition, the coupling between the two hydrogen bonded OH stretches in the hydronium core is roughly twice the size of the coupling between one of these vibratoins and the free OH stretch. The latter coupling being comparable in size to that in hydronium. This reflects the fact that as one of the hydrogen-bonded OH bonds is elongated, the system moves from the symmetric trimer structure shown in Figure 2 to a structure that more closely

resembles that of $H_5O_2^+$ solvated by a water molecule. This would lead to an elongation of the OH bond length for the shared proton in the nascent $H_5O_2^+$ and a shortening of the bond length of the other shared proton OH bond.

Similar trends are also seen in $H_9O_4^+$ although the magnitudes of the couplings are generally smaller than in $H_7O_3^+$. Most notably, the coupling between the OH stretches in the hydronium core are roughly half those in bare hydronium. As discussed previously,[23] the supression of these couplings reflects the fact that in this configuration the OH bonds are lower frequency and more anharmonic than in an isolated hydronium ion. As a result, a smaller force is required to relax the other OH bond lengths as one of the OH bonds in the hydronium core is elongated, and the system is driven toward a hydronium ion solvated by $(H_2O)_3$.

In Table S4, we report the harmonic and anharmonic frequencies and intensities for the OH stretches, evaluated at the MP2/aug-cc-pVTZ level of theory and basis using VPT2 as implemented in Gaussian 16.[47,54] These are compared to the anharmonic frequencies and intensities of the corresponding transitions, evaluated by applying second order degenerate perturbation theory to the harmonically coupled anharmonic oscillator model. In general the anharmonic frequencies evaluated by the two approaches are in good agreement, differing by several tens of cm^{-1}. These differences reflect the neglect of couplings to other vibrational degrees of freedom. These couplings are particularly notable for the shared proton stretches in $H_7O_3^+$, which will be explored further in the following section. The intensities calculated using the HCAO model more closely resemble the harmonic intensities from the electronic structure calculation. Some of the differences between the VPT2 intensities and those from the HCAO model reflect the fact there is a problem with symmetry breaking in the VPT2 calculations. In the case of the shared proton stretch the higher intensity from the HCAO model calculations also reflects the absence of coupling between these states and overtones and combination bands involvong lower frequency vibrations.

Higher order couplings in $H_7O_3^+$

Having explored how couplings are encoded in the harmonic analysis of protonated water clusters, we turn our attention to the results of VPT2 applied to $H_7O_3^+$. We choose this system because VPT2 brakes down catastrophically for $H_5O_2^+$ due to the very flat potential along the shared proton stretch coordinate as well as the large couplings between the shared proton stretch and other vibrational degrees of freedom.[16] In contrast, VPT2 appears to work reasonably well for $H_9O_4^+$.[15] In Figure 5 we plot the VPT2 spectra evaluated in an internal coordinate representation, described above, when resonance interactions are included and when they have not been considered. These spectra are compared to the spectrum of this ion obtained by argon detachment.[55] When resonances are included, we use degenerate VPT2 to develop a reduced dimensional Hamiltonian that includes only those states that are strongly coupled to the shared proton stretches. The resulting 17×17 matrix is diagonalized. This degenerate perturbation theory approach removes problems often associated with small denominators.

As can be seen in the plots in Figure 5 and in the numerical information provided in Tables S5 - S7, when near degeneracies are not accounted for both the shared proton stretch and the bend at 1500 cm^{-1} have unphysically large intensities relative to other transitions. By removing the terms by the Hamiltonian that couple nearly degenerate states from the perturbation theory analysis the breadth of the feature that spans 1700 to 2700 cm^{-1} in the measured spectrum is captured, although the details of this feature are not fully reproduced. Likewise, the peaks near 1500 to 1600 cm^{-1} contain substantially less intensity than is observed. By employing degenerate perturbation theory, we are now able to analyze the contributions to these states. We find that the zero-order bright states in this spectral region, the in- and out-of-phase shared protons stretches, each contribute to a number of eigenstates. The extent of the mixing of zero-order states is quantified by the results reported in Table S7. Looking at the zero-order states that contribute to the transitions that have significant intensity, we find that most involve overtones and combination bands that correspond to

internal rotation and tunneling of the hydronium core, as illustrated in the inset in Figure 5(b). These are the types of motions that would break the strong hydrogen bonds between the hydronium core and the flanking water molecules. As the OH bond lengths in the hydronium core in $H_7O_3^+$ are 1.04 Å, while they are 0.979 Å in isolated hydronium (see Table 1), motions that break the hydrogen bonding network are anticipated to be strongly coupled to the shared proton stretch. In addition, earlier studies of ion-water complexes showed that overtones of vibrations that break the hydrogen bond can have surprisingly large intensity in the absence of coupling to other zero-order bright states.[56] At the harmonic level, these vibrations have frequencies ranging from 1150 to 1275 cm^{-1}, which is roughly half the frequency of the shared proton stretch. The above factors set up the system for strong 2:1 Fermi resonance interactions.

In addition, combination bands involving the shared proton stretch and the OO stretch are expected to have substantial intensities through mechanisms previously explored for Ar·HCOH[57] and hydronium solvated in a crown ether cage.[23] In this case, the mechanism by which these transitions gain intensity requires the consideration of an adiabatic picture in which the minimum in an effective potential along the OO stretch coordinate shifts to shorter distances as the OH bond is excited. This can be attributed to an increase in the hydrogen bond strength and a decrease in the OH vibrational frequency as the OO distance is decreased. By analogy to the Franck-Condon picture used to interpret electronic spectra, this shift in the minimum of the adiabatic potential along the OH bond coordinate leads to a progression in the OO stretch vibration built off of the shared proton stretch fundamental.[23] In all, despite being a highly anharmonic system, VPT2 can provide insights into the nature and consequences of couplings in $H_7O_3^+$.

Summary and Conclusions

In this study, we have explored several of the mechanisms for coupling in protonated water clusters, focusing on systems with four or fewer water molecules. We find that even at the harmonic level, couplings between the shared proton stretch and the HOH bends have a notable effect on the spectra for $H_5O_2^+$ and $H_7O_3^+$. While this analysis was based on harmonic treatments, the validity of the approach required much more sophisticated treatments of the molecular vibrations. In particular, evaluation of the ground state probability amplitude using Diffusion Monte Carlo allowed us to recognize that for all of these systems there is significant amplitude at the transition states shown in Figure 2. This insight allowed us to focus our analysis of these couplings on the transition state structures, where symmetry simplified the picture considerably. We also explored the nature of anharmonic couplings in $H_7O_3^+$ using a degenerate variant of VPT2, performed in terms of normal modes that are linear combinations of internal, rather than Cartesian, coordinates. This analysis allowed us to obtain a better understanding of the types of states that are coupled to the zero-order bright shared proton stretches. While the above discussion focused on the protonated water systems, it serves to illustrate ways in which one can couple various theoretical and computational approaches to obtain a deeper understanding of the nature of couplings in highly anharmonic systems more generally.

Acknowledgement

Support from the Chemistry Division of the National Science Foundation (CHE-1619660) is gratefully acknowledged. This work was supported in part by allocations of computing time from the Ohio Supercomputer Center to A.B.M. and L.C.D.. Parts of this work were performed using the Ilahie cluster, which was purchased using funds from a MRI grant from the National Science Foundation (CHE-1624430).

References

(1) de Grotthuss, C. J. T. Theory of Decomposition of Liquids by Electrical Currents. *Ann. Chim. (Paris)* **1806**, *LVIII*, 54– 74.

(2) Marx, D.; Tuckerman, M. E.; Hutter, J.; Parrinello, M. The Nature of the Hydrated Excess Proton in Water. *Nature* **1999**, *397*, 601 –604.

(3) Hynes, J. T. The Protean Proton in Water. *Nature* **1999**, *397*, 565 – 567.

(4) Berkelbach, T. C.; Lee, H.-S.; Tuckerman, M. E. Concerted Hydrogen-Bond Dynamics in the Transport Mechanism of the Hydrated Proton: A First-Principles Molecular Dynamics Study. *Phys. Rev. Lett.* **2009**, *103*, 238302.

(5) Markovitch, O.; Chen, H.; Izvekov, S.; Paesani, F.; Voth, G. A.; Agmon, N. Special Pair Dance and Partner Selection: Elementary Steps in Proton Transport in Liquid Water. *J. Phys. Chem. B* **2008**, *112*, 9456–9466.

(6) Knight, C.; Voth, G. A. The Curious Case of the Hydrated Proton. *Acc. Chem. Res.* **2012**, *45*, 101–109.

(7) Okumura, M.; Yeh, L. I.; Myers, J. D.; Lee, Y. T. Infrared Spectra of the Cluster Ions $H_7O_3^+ \cdot H_2$ and $H_9O_4^+ \cdot H_2$. *J. Chem. Phys.* **1986**, *85*, 2328–2329.

(8) Yeh, L. I.; Okumura, M.; Myers, J. D.; Price, J. M.; Lee, Y. T. Vibrational spectroscopy of the hydrated hydronium cluster ions $H_3O^+ \cdot (H_2O)_n$ (n = 1, 2, 3). *J. Chem. Phys.* **1989**, *91*, 7319–30.

(9) Yeh, L. I.; Lee, Y. T.; Hougen, J. T. Vibration-rotation spectroscopy of the hydrated hydronium ions $H_5O_2^+$ and $H_9O_4^+$. *J. Mol. Spect.* **1994**, *164*, 473–88.

(10) Headrick, J. M.; Diken, E. G.; Walters, R. S.; Hammer, N. I.; Christie, R. A.; Cui, J.; Myshakin, E. M.; Duncan, M. A.; Johnson, M. A.; Jordan, K. D. Spectral Signatures of Hydrated Proton Vibrations in Water Clusters. *Science* **2005**, *308*, 1765069.

(11) Douberly, G. E.; Walters, R. S.; Cui, J.; Jordan, K. D.; Duncan, M. A. Infrared Spectroscopy of Small Protonated Water Clusters, $H^+(H_2O)_n$ ($n = 25$): Isomers, Argon Tagging, and Deuteration. *J. Phys. Chem. A* **2010**, *114*, 4570–4579.

(12) Mizuse, K.; Fujii, A. Tuning of the Internal Energy and Isomer Distribution in Small Protonated Water Clusters $H^+(H_2O)_{4-8}$: An Application of the Inert Gas Messenger Technique. *J. Phys. Chem. A* **2012**, *116*, 4868–4877.

(13) Fournier, J. A.; Wolke, C. T.; Johnson, M. A.; Odbadrakh, T. T.; Jordan, K. D.; Kathmann, S. M.; Xantheas, S. S. Snapshots of Proton Accommodation at a Microscopic Water Surface: Understanding the Vibrational Spectral Signatures of the Charge Defect in Cryogenically Cooled $H^+(H_2O)_{n=2-28}$ Clusters. *J. Phys. Chem A* **2015**, *119*, 9425–9440.

(14) Thämer, M.; De Marco, L.; Ramasesha, K.; Mandal, A.; Tokmakoff, A. Ultrafast 2D IR Spectroscopy of the Excess Proton in Liquid Water. *Science* **2015**, *350*, 78–82.

(15) Wolke, C. T.; Fournier, J. A.; Dzugan, L. C.; Fagiani, M. R.; Odbadrakh, T. T.; Knorke, H.; Jordan, K. D.; McCoy, A. B.; Asmis, K. R.; Johnson, M. A. Spectroscopic Snapshots of the Proton-Transfer Mechanism in Water. *Science* **2016**, *354*, 1131–1135.

(16) Hammer, N. I.; Diken, E. G.; Roscioli, J. R.; Myshakin, E. M.; Jordan, K. D.; McCoy, A. B.; Huang, X.; Carter, S.; Bowman, J. M.; Johnson, M. A. The Vibrational Predissociation Spectra of the $H_5O_2^+ \cdot RG_n$ (RG = Ar, Ne) Clusters: Correlation of the Solvent Perturbations in the Free OH and Shared Proton Transitions of the Zundel Ion. *J. Chem. Phys.* **2005**, *123*, 044308.

(17) Vendrell, O.; Gatti, F.; Meyer, H.-D. Strong Isotope Effects in the Infrared Spectrum of the Zundel Cation. *Agew. Chem. Int. Ed.* **2009**, *48*, 352–355.

(18) Bykov, A.; Makushkin, Y.; Ulenikov, O. The Vibrational Analysis of $H_2{}^{16}O$. *J. Mol. Spectrosc.* **1983**, *99*, 221 – 227.

(19) Begemann, M. H.; Gudeman, C. S.; Pfaff, J.; Saykally, R. J. Detection of the Hydronium Ion (H_3O^+) by High-Resolution Infrared Spectroscopy. *Phys. Rev. Lett.* **1983**, *51*, 554–557.

(20) Duong, C. H.; Gorlova, O.; Yang, N.; Kelleher, P. J.; Johnson, M. A.; McCoy, A. B.; Yu, Q.; Bowman, J. M. Disentangling the Complex Vibrational Spectrum of the Protonated Water Trimer, $H^+(H_2O)_3$, with Two-Color IR-IR Photodissociation of the Bare Ion and Anharmonic VSCF/VCI Theory. *J. Phys. Chem. Lett.* **2017**, *8*, 3782–3789.

(21) McCunn, L. R.; Roscioli, J. R.; Johnson, M. A.; McCoy, A. B. An H/D Isotopic Substitution Study of the $H_5O_2^+\cdot$ Ar Vibrational Predissociation Spectra: Exploring the putative Role of Fermi Resonances in the Bridging Proton Fundamentals. *J. Phys. Chem. A* **2008**, *112*, 321–327.

(22) Johnson, C. J.; Dzugan, L. C.; Wolk, A. B.; Leavitt, C. M.; Fournier, J. A.; McCoy, A. B.; Johnson, M. A. Microhydration of Contact Ion Pairs in $M^{2+}OH^-(H_2O)_{n=1-5}$ (M = Mg, Ca) Clusters: Spectral Manifestations of a Mobile Proton Defect in the First Hydration Shell. *J. Phys. Chem. A* **2014**, *118*, 7590–7597.

(23) Craig, S. M.; Menges, F. S.; Duong, C. H.; Denton, J. K.; Madison, L. R.; McCoy, A. B.; Johnson, M. A. Hidden Role of Intermolecular Proton Transfer in the Anomalously Diffuse Vibrational Spectrum of a Trapped Hydronium Ion. *PNAS* **2017**, *114*, E4706–E4713.

(24) Wilson, E. B.; Decius, J. C.; Cross, P. C. *Molecular Vibrations*; Dover: New York, 1955.

(25) Quade, C. R. Internal Coordinate Formulation for the Vibration–Rotation Energies of Polyatomic Molecules. *J. Chem. Phys.* **1976**, *64*, 2783–2795.

(26) Sibert, E. L. Theoretical Studies of Vibrationally Excited Polyatomic Molecules Using Canonical Van Vleck Perturbation Theory. *J. Chem. Phys.* **1988**, *88*, 4378–4390.

(27) McCoy, A. B.; Sibert, E. L. Perturbative Calculations of Vibrational (J=0) Energy Levels of Linear Molecules in Normal Coordinate Representations. *J. Chem. Phys.* **1991**, *95*, 3476–87.

(28) Frederick, J. H.; Woywod, C. General Formulation of the Vibrational Kinetic Energy Operator in Internal Bond-Angle Coordinates. *J. Chem. Phys.* **1999**, *111*, 7255–7271.

(29) Child, M. S.; Lawton, R. T. Local and Normal Vibrational States: a Harmonically Coupled Anharmonic Oscillator Model. *Faraday Discuss. Chem. Soc.* **1981**, *71*, 273–85.

(30) Lehmann, K. K. On the Relation of Child and Lawton's Harmonically Coupled Anharmonic–Oscillator Model and Darling–Dennison Couplings. *J. Chem. Phys.* **1983**, *79*, 1098–1098.

(31) Mills, I.; Robiette, A. On the Relationship of Normal Modes to Local Modes in Molecular Vibrations. *Mol. Phys.* **1985**, *56*, 743–765.

(32) Roberts, M. A.; Savage, C.; Dong, F.; Sharp-Williams, E. N.; McCoy, A. B.; Nesbitt, D. J. Sub-Doppler Infrared Spectroscopy of CH_2D Radical in a Slit Supersonic Jet: Isotopic Symmetry Breaking in the CH Stretching Manifold. *J. Chem. Phys.* **2012**, *136*, 234308.

(33) Hsu, K.-H.; Huang, Y.-H.; Lee, Y.-P.; Huang, M.; Miller, T. A.; McCoy, A. B. Manifestations of Torsion-CH Stretch Coupling in the Infrared Spectrum of CH_3OO. *J. Phys. Chem A* **2016**, *0*, null.

(34) Huang, M.; Miller, T. A.; McCoy, A. B.; Hsu, K.-H.; Huang, Y.-H.; Lee, Y.-P. Modeling the CH Stretch/Torsion/Rotation Couplings in Methyl Peroxy (CH_3OO). *J. Phys. Chem. A* **2017**, *121*, 9619–9630.

(35) Sibert, E. L.; Tabor, D. P.; Kidwell, N. M.; Dean, J. C.; Zwier, T. S. Fermi Resonance Effects in the Vibrational Spectroscopy of Methyl and Methoxy Groups. *J. Phys. Chem A* **2014**, *118*, 11272–11281.

(36) Nielsen, H. H. The Vibration-Rotation Energies of Molecules. *Rev. Mod. Phys.* **1951**, *23*, 90–136.

(37) Martin, J. M. L.; Lee, T. J.; Taylor, P. R.; François, J. The Anharmonic Force Field of Ethylene, C_2H_4, by Means of Accurate ab Initio Calculations. *J. Chem. Phys.* **1995**, *103*, 2589–2602.

(38) Dzugan, L. C.; Matthews, J.; Sinha, A.; McCoy, A. B. Role of Torsion-Vibration Coupling in the Overtone Spectrum and Vibrationally Mediated Photochemistry of CH_3OOH and HOOH. *J. Phys. Chem A* **2017**, *121*, 9262–9274.

(39) Dzugan, L. C. Theoretical Treatments of the Effects of Low Frequency Vibrations on OH Stretches in Molecules and Ion-Water Complexes That Undergo Large Amplitude Motions. Ph.D. thesis, The Ohio State University, 2017.

(40) Anderson, J. B. A Random-Walk Simulation of the Schrödinger Equation: H_3^+. *J. Chem. Phys.* **1975**, *63*, 1499–1503.

(41) Anderson, J. B. Quantum Chemistry by Random Walk. H ^2P, H_3^+ D_{3h} $^1A_1'$, H_2 $^3\Sigma_u^+$, H_4 $^1\Sigma_g^+$, Be ^1S. *J. Chem. Phys.* **1976**, *65*, 4121–4127.

(42) Suhm, M. A.; Watts, R. O. Quantum Monte Carlo Studies of Vibrational States in Molecules and Clusters. *Physics Reports* **1991**, *204*, 293–329.

(43) McCoy, A. B. Diffusion Monte Carlo for Studying Weakly bound Complexes and Fluxional Molecules. *Int. Rev. in Phys. Chem.* **2006**, *25*, 77–108.

(44) Petit, A. S.; Wellen, B. A.; McCoy, A. B. Unraveling Rotation-Vibration Mixing in

Highly Fluxional Molecules Using Diffusion Monte Carlo: Applications to H_3^+ and H_3O^+. *J. Chem. Phys.* **2012**, *136*, 074101/1–12.

(45) Barnett, R.; Reynolds, P.; Lester, W. Monte Carlo Algorithms for Expectation Values of Coordinate Operators. *J. Comput. Phys.* **1991**, *96*, 258 – 276.

(46) Yu, Q.; Bowman, J. M. Communication: VSCF/VCI Vibrational Spectroscopy of $H_7O_3^+$ and $H_9O_4^+$ Using High-Level, Many-Body Potential Energy Surface and Dipole Moment Surfaces. *J. Chem. Phys.* **2017**, *146*, 121102.

(47) Frisch, M. J.; Trucks, G. W.; Schlegel, H. B.; Scuseria, G. E.; Robb, M. A.; Cheeseman, J. R.; Scalmani, G.; Barone, V.; Petersson, G. A.; Nakatsuji, H. et al. Gaussian16 Revision A.03. 2016; Gaussian Inc. Wallingford CT.

(48) Frisch, M. J.; Trucks, G. W.; Schlegel, H. B.; Scuseria, G. E.; Robb, M. A.; Cheeseman, J. R.; Scalmani, G.; Barone, V.; Mennucci, B.; Petersson, G. A. et al. Gaussian09 Revision D.01. Gaussian, Inc., Wallingford, CT 2009.

(49) Huang, X.; Braams, B. J.; Bowman, J. M. *Ab initio* Potential Energy and Dipole Moment Surfaces for $H_5O_2^+$. *J. Chem. Phys.* **2005**, *122*, 044308.

(50) Dong, F.; Nesbitt, D. J. Jet Cooled Molecular Ions in Slit Supersonic Discharges: High Resolution Infrared Studies of Hyrdronium Ion Isotopomers in the OD stretch regionooled spectroscopy of H_2DO^+: Barrier heights and Isotope-Dependent Tunneling Dynamics From H_3O^+ to D_3O^+. *J. Chem. Phys.* **2006**, *125*, 144311.

(51) McCoy, A. B.; Huang, X.; Carter, S.; Landeweer, M. Y.; Bowman, J. M. Full-Dimensional Vibrational Calculations for $H_5O_2^+$ Using an *ab initio* Potential Energy Surface. *J. Chem. Phys.* **2005**, *122*, 061101/1–4.

(52) Guasco, T. L.; Johnson, M. A.; McCoy, A. B. Unraveling Anharmonic Effects in the

Vibrational Predissociation Spectra of $H_5O_2^+$ and its Deuterated Analogues. *J. Phys. Chem. A* **2011**, *115*, 5847–5858.

(53) McCoy, A. B.; Leavitt, C. M.; Guasco, T. L.; Olsen, S. G.; Johnson, M. A. Vibrational Manifestations of Strong Non-Condon Effects in the $H_3O^+ \cdot X_{1-3}$ (X=Ar, N_2, CH_4, H_2O) Complexes: Microscopic Analogues of the Association Band in the Vibrational Spectrum of Water. *Phys. Chem. Chem. Phys.* **2012**, *14*, 7205–7214.

(54) Barone, V. Anharmonic Vibrational Properties by a Fully Automated Second-Order Perturbative Approach. *J. Chem. Phys.* **2005**, *122*, 014108/1–10.

(55) Relph, R. A.; Guasco, T. L.; Elliott, B. M.; Kamrath, M. Z.; McCoy, A. B.; Steele, R. P.; Schofield, D. P.; Jordan, K. D.; Viggiano, A. A.; Ferguson, E. E. et al. How the Shape of an H-Bonded Network Controls Proton-Coupled Water Activation in HONO Formation. *Science* **2010**, *327*, 308–12.

(56) Roscioli, J. R.; Diken, E. G.; Johnson, M. A.; Horvath, S.; McCoy, A. B. Prying Apart a Water Molecule with Anionic H-Bonding: A Comparative Spectroscopic Study of the $X^- \cdot H_2O$ (X=OH, O, F. Cl and Br) Binary Complexes in the 600 - 3800 cm^{-1} Region. *J. Phys. Chem. A* **2006**, *110*, 4943–52.

(57) Mauney, D. T.; Mosley, J. D.; Madison, L. R.; McCoy, A. B.; Duncan, M. A. Infrared Spectroscopy and Theory of the Formaldehyde Cation and its Hydroxymethylene Isomer. *J. Chem. Phys.* **2016**, *145*, 174303.

Table 1: Structural parameters and frequencies of water and protonated water clusters with one to four water molecules. All calculated values are obtained at the MP2/aug-cc-pVTZ level of theory/basis.

system	r_e^{OH}	θ_e^{HOH}	ν_{ss} (calc)	ν_{as} (calc)	ν_{HOH} (calc)	ν_{ss} (obs)	ν_{ss} (obs)	ν_{HOH} (obs)	ν_{IHB} (obs)	r_e^{IHB}
HOH [a]	0.9614	104.1	3654	3768	1578	3657	3756	1595		
H_3O^+ [b]	0.9795	111.5	3410	3502	1625	3445	3536	1626		
$H_5O_2^+$ [c]	0.9684	108.8	3571 [d]	3657 [d]	1847	3603	3683	1763	1047	1.1972
$H_7O_3^+$ [e]	0.9642	114.6	≈3600 [d]	3721 [d]	1552	3640	3726	1534		1.0374
		106.9			1635			1639		
$H_9O_4^+$ [f]	0.9636	112.6	3622 [d]	3711	1539	3648	3733	1615	2653	1.0110

[a] .[18]

[b] Values reflect lower energy member of the tunneling doublet.[49]

[c] Based on Ne-tagged spectrum.[16,17]

[d] The VPT2 calculation broke the degeneracy of these vibrations and the reported values are the average of the calculated results.

[e] Based on D_2-tagged spectrum.[20]

[f] Based on D_2-tagged spectrum.[15]

Table 2: Calculated kinetic and potential stretch/bend coupling in the protonated water clusters.

	uncoupled[a]			coupling[b]		coupled[c]	
system	OH	HOH (water)	HOH (hydronium)	Pot	Kin	OH	HOH[d]
HOH	3810	1641		-380	144	3803	1622
H_3O^+	3785		1629	47	-214	3886	1623
	3785		1629	0	-214	3889	1622
$H_5O_2^+$	1017		1616	748	63	747	1778
	1017		1616	748	0	762	1744
$H_7O_3^+$ - asym[e]	2451		1636	-201	-160	2505	1552
		1641		-291	0		1656
	2451		1636	-201	0	2478	1570
		1641		-291	0		1651
$H_7O_3^+$ - sym[e]	2617		1638	-141	-83	2635	1597
		1645		-231	0		1644
	2617		1638	-141	0	2630	1603
		1645		-231	0		1646
$H_9O_4^+$ - asym[e]	2966		1655	110	172	2985	1601
		1640		-216	0		1657
	2966		1655	110	0		1607
		1640		-216	0		1662
$H_9O_4^+$ - sym[e]	3022	1645		162	0	3025	1628

[a] Frequencies evaluated based on symmetry adapted linear combinations of equivalent OH bond lengths/HOO angles.
[b] Harmonic couplings between uncoupled vibrations.
[c] Frequencies evaluated based on a FG analysis of the uncoupled states including only OH stretches and HOH bends.
[d] In $H_7O_3^+$ and $H_9O_4^+$ the bends are highly mixed in character and are reported in order of increasing frequency.
[e] In $H_7O_3^+$ and $H_9O_4^+$ the stretch/bend couplings is divided into symmetry blocks.

Table 3: Calculated kinetic and potential stretch/bend coupling in the deuterated variants of $H_5O_2^+$.

	uncoupled[a]		coupling[b]		coupled[c]	
system	OH	HOH	Pot	Kin	OH	HOH[d]
$H^+(H_2O)_2$	1017	1616	748	63	747	1778
	1017	1616	748	0	762	1744
$H^+(D_2O)_2$	1017	1188	641	74	678	1432
	1017	1188	641	0	702	1391
$D^+(H_2O)_2$	730	1616	634	75	558	1705
	730	1616	634		570	1673
$D^+(D_2O)_2$	730	1188	-544	-87	528	1317
	730	1188	-544	0	549	1276

[a] Frequencies evaluated based on symmetry adapted linear combinations of equivalent OH bond lengths/ HOO angles.
[b] Harmonic couplings between uncoupled vibrations.
[c] Frequencies evaluated based on a FG analysis of the uncoupled states including only OH stretches and HOH bends.

Table 4: Calculated coupling matrix elements among the OH stretches in the protonated water clusters).

system	HOH[a]	H_3O[b]	HOH/H_3O[c]
H_2O	62.9		
H_3O^+		36.5	
$H_5O_2^+$	53		98
$H_7O_3^+$	54	78.5[d]	25.5
		35[e]	
$H_9O_4^+$	54	30	17

[a] Coupling between two OH stretches in water.
[b] Coupling between two OH stretches in the hydronium core.
[c] Coupling between the IHB OH stretch and an OH stretch in water.
[d] Coupling between the two IHB OH stretches.
[e] Coupling between an IHB OH stretch and the unbound OH stretch.

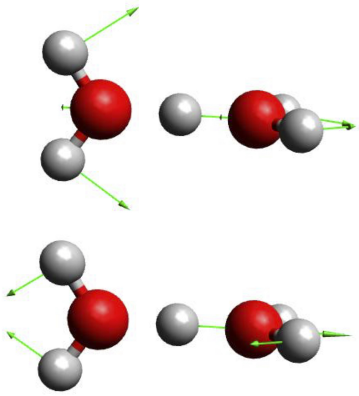

Figure 1: Two normal modes in $H_5O_2^+$, defined as linear combinations of Cartesian displacements. These are the normal modes that correspond to the out-of-phase HOH bends of the flanking water molecules (upper) and the shared proton stretch (lower).

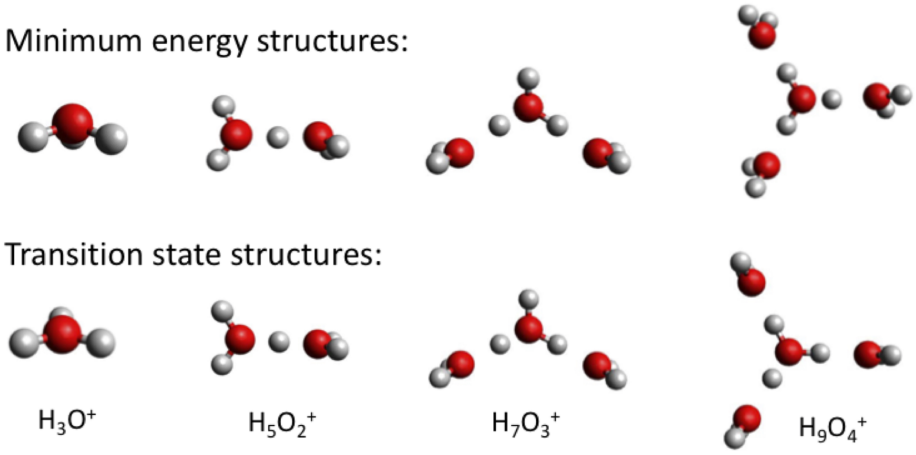

Figure 2: The equilibrium (upper) and transition state (lower) structures of protonated water clusters, $H^+ \cdot (H_2O)_n$ with $n = 1$ to 4.

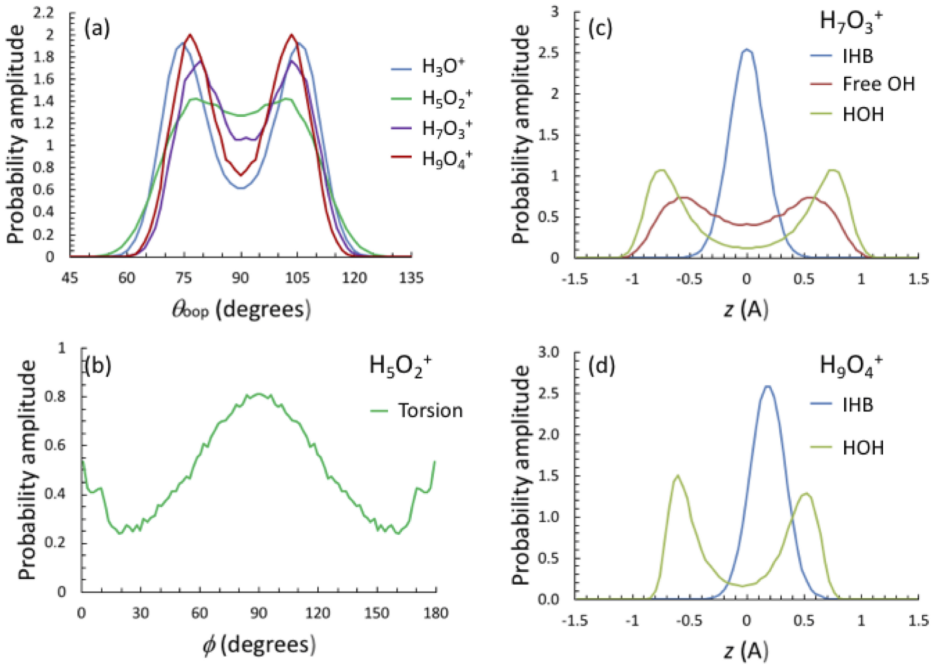

Figure 3: Projections of the ground state probability amplitude of for the the protonated water clusters onto (a) the umbrella coordinate, θ_{oop} shown in Figure 4, (b) the torsion of the two terminal water molecules in $H_5O_2^+$ and (c) and (d) the displacements of the hydrogen atoms off of the plane defined by three of the oxygen atoms in $H_7O_3^+$ and $H_9O_4^+$, as described in the text.

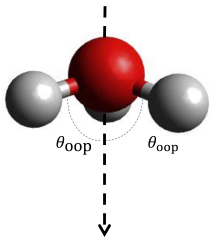

Figure 4: Definition of θ_{oop} for H_3O^+.

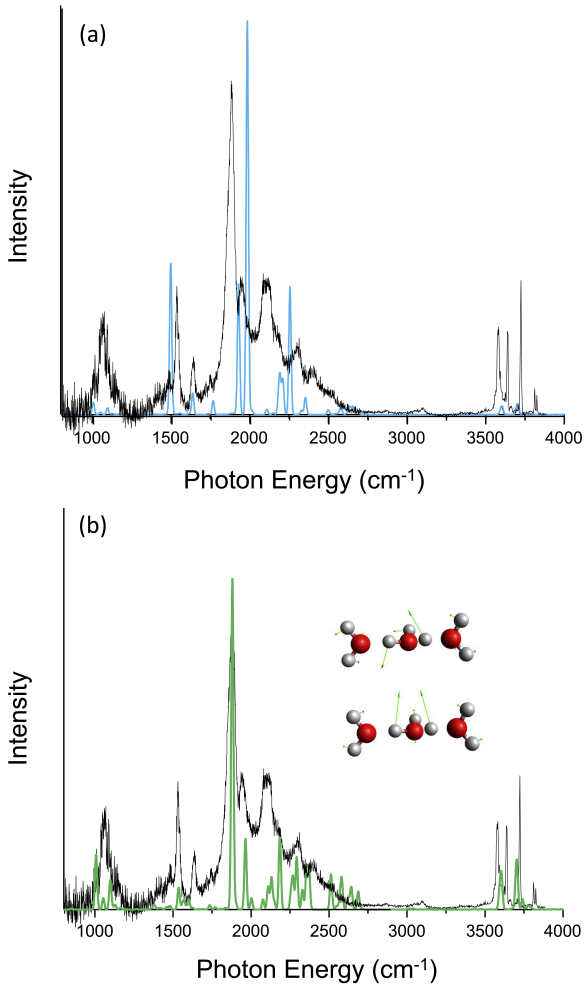

Figure 5: Observed[55] and calculated spectrum for $H_7O_3^+$. In (a) VPT2 is used to calculate the spectrum without consideration of near-degeneracies, while degenerate VPT2 is used to obtain the spectrum in (b).